Supplementary Information

Structures of a P4-ATPase lipid flippase in lipid bilayers

Yilin He[1,2], Jinkun Xu[1], Xiaofei Wu[1], Long Li[1]#

[1] State Key Laboratory of Membrane Biology, Peking-Tsinghua Center for Life Sciences, School of Life Sciences, Peking University, Beijing, China

[2] Academy for Advanced Interdisciplinary Studies, Peking University, Beijing, China

Corresponding author: Long Li; email: long_li@pku.edu.cn

Contents

Supplemental results and discussion

Results

In both E1-ATP and E2P structures, ctCdc50p has extensive interactions with ctDnf1p. On the cytoplasmic side, the N-terminal peptide (residues 23-46) of ctCdc50p runs along one face of ctDnf1p, interacting with the cytosolic loops of ctDnf1p, including the segment connecting TM4 and the P domain, the loop between TMs 6 and 7 (L6/7), L8/9, and a C-terminal amphipathic helix that was suggested to undergo conformational changes upon PI4P activation in scDrs2p[1,2] (Fig. S10). The C-terminal tail of ctCdc50p (residues 384-398), which is invisible in the scCdc50p and hCDC50a structures, could be traced to run towards ctDnf1p. Thus, the C-terminal tail and the N-terminal peptide of ctCdc50p are in such a conformation that sandwiches the C-terminal amphipathic helix of ctDnf1p (Fig. S10). The two TMs of ctCdc50p form hydrophobic interactions with TM7 and TM10 of ctDnf1p. The ectodomain of ctCdc50p has the largest interfaces with ctDnf1p, interacting with all the exoplasmic loops except L1/2 (Fig. 1a). Thus, ctCdc50p acts as a 3-way clamp to hold TMs 3-10 of ctDnf1p in a relatively fixed conformation in both E1-ATP and E2P structures.

The E1-ATP and E2P structures have a lipid-binding site in common in a cavity formed by TMs 7, 8, and 10, on the opposite side of TMs 2, 4, and 6 (Fig. S11). Phospholipid density is observed at the cytoplasmic border of the membranes. The cavity was suggested to be a PI4P binding site for scDrs2p activation[1]. However, in our structures, the head group does not insert as deep as PI4P in scDrs2p $E2P^{inter}$ or $E2P^{active}$. Instead, it is likely to be the head group of PS as modeled in scDrs2p $E2P^{inhib\ 1}$.

Discussion

Phospholipid flipping coupled with the E1-E2 transition

Four lipid-binding sites are identified in the groove formed by TMs 2, 4, and 6, two from E1-ATP and two from E2P. The four sites arranged in such a way that they could relay the phospholipid substrates through the groove during the E1-E2 transition (Fig. S12). Conformational changes of TM1 and TM2 guide the phospholipids to move from the exoplasmic leaflet to the cytoplasmic leaflet. ATP binding to the lipid flippase in the E1-ATP state detaches the A domain from the N and P domains. The large motion of the A domain increases the flexibility of TMs 1 and 2 and exposes a negatively charged patch formed by the residues from TMs 2 and 4. The local lipid bilayers are distorted and the membranes are thinned by almost a half. In the distorted membranes, the phospholipid molecules are more likely to tilt parallel to the

membrane plane. The lipid head groups are in an inward-facing orientation, ready to enter the groove via E1-site2 (Fig. S12a). In the E2P state, the A domain is associated with the P and N domains tightly, leading to a relatively rigid conformation of TMs 1 and 2. The local lipid bilayer structures are restored. TMs 2, 4, and 6 create a cavity (E2-site1) in the exoplasmic leaflet for shielding the polar head group of the phospholipid that has been picked up from E1-site2 (Fig. S12b). E2-site1 is disrupted in the E1-ATP state as TM2 moves towards TMs 4 and 6 and two polar residues of TM4 (Q549 and N550) lean towards the membranes. The lipid head group is likely to be squeezed out and to move forward to the cytoplasmic leaflet via E1-site1, a shallow hydrophilic cleft (Fig. S12c). Finally, the phospholipid reaches E2-site2 and is held by a clamp between TMs 2 and 4 in a flipped conformation (Fig. S12d). The phospholipid substrate is ready to be laterally released into the cytoplasmic leaflet when the clamp is disrupted in the E1-ATP state. In the scenario proposed above, it takes two E1-E2 cycles to flip one phospholipid substrate, but costs one ATP molecule per phospholipid on average because two phospholipids are present at the same time in each state. However, as we are missing several intermediate states, e.g. E2 and E1P, the exact cycle number and ATP cost per substrate need further investigation. During lipid transport, the hydrophilic head group of the phospholipid substrate is constantly protected from the hydrophobic environment by sliding through the binding sites in the positively charged groove (Fig. 2b, d). The groove provides the only continuous hydrophilic pathway in the M domain during the E1-E2 transition (Compare Fig. 2b, d and Fig. S11c). The positive charges are mainly contributed by K174, R181, and K1121 on the TMs. The highly conserved K1121 has been shown to be important for substrate binding and ATPase activity[3]. Consistent with biochemical data[3], the groove has high affinity to the lipid substrate in the E2P state as evident by the strong phospholipid density, whereas the groove shows weak lipid binding to facilitate lipid entry and exit in the E1-ATP state as indicated by the fragmented lipid density in the structure. Similarly, a hydrophilic membrane-traversing groove is also present in the TMEM16F scramblase[4].

The “hydrophobic gate” model suggests that TMs 1 and 2 move away from TMs 3 and 4 during lipid transport[5]. Indeed, our structures show that TM1 and TM2 becomes flexible in E1-ATP. The key residue, I364 of the “hydrophobic gate” (I554 in ctDnf1p), is at the interface between TMs 1, 2, and 4 (Fig. S13). Thus the mutations of the residue may disrupt the E1-E2 equilibrium and hamper lipid flipping as observed in the mutagenesis studies[5]. The “two-gate” model suggests that the flippases recognize the phospholipid substrates by interacting with the head groups. Residues other than the classical ion binding residues in ion-pumping P-type ATPases are involved in recognition[6-9]. Consistent with the model, the four distinct binding sites in our structures mainly interact with the lipid head groups. However, the sites do not seem to provide a discrimination mechanism for different phospholipid substrates. As shown in the phospholipid-dependent ATPase activity assays, ctDnf1p may have different

substrate specificity from scDrs2p and hATP8A1. The amino acids that interact with the polar head group of the phospholipid substrate at E2-site1 are similar to those in the structures of scDrs2p and hATP8A1. The corresponding residues are Q549 and N550 of ctDnf1p, S503 and N504 of scDrs2p, and N352 and N353 of hATP8A1 (Fig. S1). The clamp residues of E2-site2 consist of both hydrophilic and hydrophobic residues, but are not conserved among P4-ATPases (Fig. S1). The serine residues at E1-site1 are highly conserved among P4-ATPases, and E1-site2 only provides a steric opening. Further studies on other intermediate states may provide clues on the substrate specificity.

Materials and methods

Protein expression and purification

Protein BLAST search identified three P4-ATPases in *C. thermophilum*, including one *S. cerevisiae* Drs2p homolog (ctDrs2p), one Dnf1p and Dnf2p homolog (ctDnf1p), and one Dnf3p homolog (ctDnf3p) (Fig. S1). Only one CDC50 protein was found in the *C. thermophilum* genome (ctCdc50p). After initial screening, ctDnf1p was chosen to co-express with ctCdc50p in yeast. The genes of ctDnf1p and ctCdc50p were cloned from the cDNA library of *Chaetomium thermophilum* (*var. thermophilum* strain: DSM1495, a gift from Dr. Stefan Schoebel). Superfolder green fluorescence protein (sfGFP)[10], a Twin-Strep tag and a 3C protease cleavage site were fused to the N-terminus of ctDnf1p. sfGFP, a His_9 tag, and a 3C protease cleavage site were fused to the N-terminus of ctCdc50p. The expression plasmids pRS426-sfGFP-twinStrep-3C-ct*DNF1* and pRS424-sfGFP-His_9-3C-ct*CDC50* were co-transformed into *S. cerevisiae* strain BJ5465 using the LiAc/SS carrier DNA/PEG method[11]. Yeast cells were cultured in synthetic drop-out medium supplemented with 2% raffinose at 30 °C for about 24h to reach an optical density (OD_{600}) of about 5. The culture was induced by the addition of 2% galactose and continued for 20 h at 25°C. The cells were harvested and stored at −80 °C until use.

The cells were suspended in the membrane extraction buffer (20 mM Tris-HCl pH 7.4, 150 mM NaCl, 5mM $MgCl_2$,1mM DTT, and protease inhibitor cocktails) and lysed by high pressure homogenization. The crude lysate was clarified by centrifugation (20,000×g, 25 min, 4°C). The membrane fraction was pelleted by ultracentrifugation (200,000×g, 1 h, 4°C) and washed once with the membrane extraction buffer. The membrane pellets were solubilized in 2% lauryl maltose neopentyl glycol (LMNG, Anatrace) in the membrane solubilization buffer (20 mM Tris-HCl pH 7.4, 150 mM NaCl, 5mM $MgCl_2$,1mM DTT, 10% glycerol, and protease inhibitor cocktails). After incubation at 4 °C for 1 h, the solution was clarified by ultracentrifugation (200,000×g, 1 h, 4°C). The supernatant was mixed with avidin (Sigma) and loaded onto a column pre-packed with StrepTactin resin (IBA

Lifesciences). The eluents were concentrated and incubated with 3C protease at 4°C overnight. The protein solution was then loaded onto a Superdex 200 10/300 column (GE Healthcare). The peak fractions were pooled and concentrated (Fig. S2). The purified protein was either reconstituted into nanodiscs or flash-frozen in liquid nitrogen and stored at −80 °C.

The purified protein was mixed with MSP1D1[12] and yeast polar lipids (Avanti Lipids, 40 mg/ml dissolved in 1% DDM) at a molar ratio of 1:2:25. Bio-beads SM2 (Bio-Rad) were then added to the mixture and incubated at 4 °C overnight to remove detergents. The complex was further purified by size-exclusion chromatography on a Superdex 200 10/300 column. The peak fraction had a protein concentration of 1.0 mg/ml (Fig. S2). It was immediately used for cryo-EM sample preparation without concentrating.

Cryo-EM sample preparation and data collection

The freshly prepared samples were incubated with 1mM BeF_3 or 1mM AMPPCP on ice for 30min before vitrification. The cryo-grid preparation was performed at 4 °C and 100% humidity in an FEI Vitrobot Mark IV. 4 μl sample was applied to each freshly glow-discharged grid (Quantifoil, R1.2/1.3). The grids were then plunge-frozen in liquid ethane. The cryo-grids were screened with a 200 kV FEI Talos Arctica microscope equipped with a FEI Ceta camera. The data were collected on a 300 kV FEI Titan Krios TEM with a K2 summit camera and GIF Quantum energy filter (Gatan). The images were collected at a magnification of 130,000× with a calibrated pixel size of 1.055 Å. The dose rate was set at 8 e^-/s/pixel and the exposure time was 8 s, corresponding to a total dose of 57.5 $e^-/Å^2$. Movie stacks (32 frames each) were recorded with the software SerialEM[13] under low-dose conditions with defocuses ranging from -1 to -2 μm.

Image processing

The movie stacks were subject to motion correction and electron-dose weighting by using MotionCor2[14] (Fig. S3a, S4a). The program Gctf[15] was used to estimate the contrast transfer function (CTF) parameters. Images of high quality were selected for further image processing on the basis of the CTF power spectra of the corrected images. The following calculations are performed with RELION3.0[16]. Particles of high quality were selected according to 2D classification (Fig. S3b, S4b) and 3D classification results. The selected particles were subject to several rounds of CTF refinement and polishing. After mask-based post-processing, the final maps had resolutions of 3.40 Å and 3.48 Å for the AMPPCP and BeF_3^- samples, respectively (Fig. S3, S4). All the resolution estimations were based on gold-standard Fourier Shell Correlation (FSC) 0.143 criteria.

The model for the E2P (BeF_3^-) structure was built manually in Coot[17], with the guidance of the scDrs2p structures. The model was refined in real space using Phenix[18]. For the model building of E1-ATP (AMPPCP), the E2P model was fit in the E1-ATP density map. Each domain is subject to rigid body refinement. Due to the local resolution limits, the A and N domains were not refined further. The rest parts of the E1-ATP model were refined in real space with Phenix. Model validation was done with MolProbity[19]. The cryo-EM maps have been deposited in the Electron Microscopy Data Bank under accession numbers 0872 (BeF_3^-) and 0873 (AMPPCP). The atomic structure coordinates have been deposited in the Protein Data Bank under the accession number 6LCP (BeF_3^-) and 6LCR (AMPPCP). All other data can be obtained from the corresponding author upon reasonable request.

ATPase activity assay

The ATPase activity assays were carried out by using BIOMOL® Green (Enzo) to measure the free phosphate concentrations. The reaction solutions consisted of 0.05mg/ml protein, 0.01% LMNG, 0.02% $C_{12}E_9$ (Anatrace), 150 mM NaCl, 20 mM HEPES-NaOH pH 7.5, 5mM $MgCl_2$, 1mM DTT, 2.5mM ATP, and lipids at the indicated concentrations. The reactions were carried out at 30 °C for 20 min, and then immediately diluted 10 times for color development. 100 µl reagent was added to 50 µl sample and the mixture was incubated at room temperature for 20 min. The absorbance at 650 nm was measured in a microplate reader (BioTek Cytation5). The phosphate concentration was determined by calibration with the phosphate standard (BML-KI102).

References

1 Timcenko, M. *et al.* Structure and autoregulation of a P4-ATPase lipid flippase. *Nature* **571**, 366-+, doi:10.1038/s41586-019-1344-7 (2019).

2 Bai, L. *et al.* Autoinhibition and activation mechanisms of the eukaryotic lipid flippase Drs2p-Cdc50p. *Nat Commun* **10**, 4142, doi:10.1038/s41467-019-12191-9 (2019).

3 Coleman, J. A., Vestergaard, A. L., Molday, R. S., Vilsen, B. & Andersen, J. P. Critical role of a transmembrane lysine in aminophospholipid transport by mammalian photoreceptor P4-ATPase ATP8A2. *Proc Natl Acad Sci U S A* **109**, 1449-1454, doi:10.1073/pnas.1108862109 (2012).

4 Brunner, J. D., Lim, N. K., Schenck, S., Duerst, A. & Dutzler, R. X-ray structure of a calcium-activated TMEM16 lipid scramblase. *Nature* **516**, 207-212, doi:10.1038/nature13984 (2014).

5 Vestergaard, A. L. *et al.* Critical roles of isoleucine-364 and adjacent residues in a hydrophobic gate control of phospholipid transport by the mammalian P4-ATPase ATP8A2. *Proc Natl Acad Sci U S A* **111**, E1334-1343, doi:10.1073/pnas.1321165111 (2014).

6 Baldridge, R. D. & Graham, T. R. Identification of residues defining phospholipid flippase substrate specificity of type IV P-type ATPases. *Proc Natl Acad Sci U S A* **109**, E290-298, doi:10.1073/pnas.1115725109 (2012).

7 Baldridge, R. D. & Graham, T. R. Two-gate mechanism for phospholipid selection and transport by type IV P-type ATPases. *Proc Natl Acad Sci U S A* **110**, E358-367, doi:10.1073/pnas.1216948110 (2013).
8 Roland, B. P. & Graham, T. R. Directed evolution of a sphingomyelin flippase reveals mechanism of substrate backbone discrimination by a P4-ATPase. *Proc Natl Acad Sci U S A* **113**, E4460-4466, doi:10.1073/pnas.1525730113 (2016).
9 Roland, B. P. *et al.* Yeast and human P4-ATPases transport glycosphingolipids using conserved structural motifs. *J Biol Chem* **294**, 1794-1806, doi:10.1074/jbc.RA118.005876 (2019).
10 Pedelacq, J. D., Cabantous, S., Tran, T., Terwilliger, T. C. & Waldo, G. S. Engineering and characterization of a superfolder green fluorescent protein. *Nat Biotechnol* **24**, 79-88, doi:10.1038/nbt1172 (2006).
11 Gietz, R. D. & Schiestl, R. H. High-efficiency yeast transformation using the LiAc/SS carrier DNA/PEG method. *Nat Protoc* **2**, 31-34, doi:10.1038/nprot.2007.13 (2007).
12 Ritchie, T. K. *et al.* Chapter 11 - Reconstitution of membrane proteins in phospholipid bilayer nanodiscs. *Methods Enzymol* **464**, 211-231, doi:10.1016/S0076-6879(09)64011-8 (2009).
13 Mastronarde, D. N. Automated electron microscope tomography using robust prediction of specimen movements. *J Struct Biol* **152**, 36-51, doi:10.1016/j.jsb.2005.07.007 (2005).
14 Zheng, S. Q. *et al.* MotionCor2: anisotropic correction of beam-induced motion for improved cryo-electron microscopy. *Nat Methods* **14**, 331-332, doi:10.1038/nmeth.4193 (2017).
15 Zhang, K. Gctf: Real-time CTF determination and correction. *J Struct Biol* **193**, 1-12, doi:10.1016/j.jsb.2015.11.003 (2016).
16 Zivanov, J. *et al.* New tools for automated high-resolution cryo-EM structure determination in RELION-3. *Elife* **7**, doi:10.7554/eLife.42166 (2018).
17 Emsley, P., Lohkamp, B., Scott, W. G. & Cowtan, K. Features and development of Coot. *Acta Crystallogr D Biol Crystallogr* **66**, 486-501, doi:10.1107/S0907444910007493 (2010).
18 Afonine, P. V. *et al.* Real-space refinement in PHENIX for cryo-EM and crystallography. *Acta Crystallogr D Struct Biol* **74**, 531-544, doi:10.1107/S2059798318006551 (2018).
19 Chen, V. B. *et al.* MolProbity: all-atom structure validation for macromolecular crystallography. *Acta Crystallogr D Biol Crystallogr* **66**, 12-21, doi:10.1107/S0907444909042073 (2010).

Supplementary Figures

Fig. S1 Sequence alignment of selected P4-ATPases.

Sequence alignment of ctDnf1p, ctDrs2p and other P4-ATPases in yeast, bovine, human, and *A. thaliana*, aligned by T-coffee[48]. The conserved domains and transmembrane helices of ctDnf1p are indicated above the sequences. The conserved residues are indicated in red letters. The amphipathic helix of TM1 is highlighted with a green bar above the alignment. The phosphorylation site of the P domain is highlighted with a green dot. The residues involved in the negatively charged patch are highlighted with red dots. The residues contribute to the positive charge of the groove are highlighted with blue dots. The residues involved in E1-site1 are highlighted with orange dots. The residues involved in E2-site1 are highlighted with magenta dots. The residues involved in E1-site2 are highlighted with purple dots. The key isoleucine residue in the hydrophobic gate model is highlighted with a grey dot. Ct, *Chaetomium thermophilum*; Sc, *Saccharomyces cerevisiae*; Bt, *Bos Taurus*; Hs, *Homo sapiens*; At, *Arabidopsis thaliana*. Uniprot accession numbers: ScDRS2, P39524; ScDNF1, P32660; ScDNF2, Q12675; BtATP8A2, C7EXK4; HsATP8A1, Q9Y2Q0; HsATP8A2, Q9NTI2; HsATP11A, P98196; HsATP11C, Q8NB49; HsATP8B1, O43520; HsATP8B2, P98198; HsATP10A, O60312; AtALA2, P98205; AtALA10, Q9LI83.

Fig. S2 Purification and characterization of the ctDnf1p-Cdc50p complex.

a, Flow chart of ctDnf1p-Cdc50p purification. **b,** Size-exclusion chromatography profile of the protein complex reconstituted into nanodiscs. The gray-shaded area (Fraction 27) was used for cryo-EM analysis. **c,** SDS-PAGE analysis of fractions from the SEC purification in **b**. **d,** ATPase activity of ctDnf1p-Cdc50p complex stimulated by phospholipids. Data points represent the mean ± SEM of at least three experiments. POPC, 1-palmitoyl-2-oleoyl-sn-glycero-3-phosphocholine. POPS, 1-palmitoyl-2-oleoyl-sn-glycero-3-phospho-L-serine.

Fig. S3 Cryo-EM single particle analysis of ctDnf1p-Cdc50p with AMPPCP

a, Representative image after motion correction. **b,** Representative results of 2D classification. **c,** Workflow of the single particle analysis. **d,** Local resolution map of the final sharpened map, shown with (left) and without (right) the nanodisc. **e,** Fourier shell correlation (FSC) curve with estimated resolution according to the gold standard.

Fig. S4 Cryo-EM single particle analysis of ctDnf1p-Cdc50p with BeF_3^-.

a, Representative image after motion correction. **b,** Representative results of 2D classification. **c,** Workflow of the single particle analysis. **d,** Local resolution map of the final sharpened map shown with (left) and without (right) the nanodisc. **e,** Fourier shell correlation (FSC) curve with estimated resolution according to the gold standard.

Fig. S5 Examples of the fit of models into the density map.

a-g, Density map and model in selected regions of each domain and TMs. Residues at the beginning and end of each polypeptide segment are indicated. **h,** Density map and model of BeF_3^-, Mg^{2+}, and D606 in the E1-ATP structure. **i,** Density map and model of AMPPCP, Mg^{2+}, and D606 in the E1-ATP structure.

Fig. S6 Comparison of ctDnf1p-Cdc50p structures in the E1-ATP and E2P states.

a, Overlay of the E1-ATP and E2P structures by superimposing TMs 3-10 of ctDnf1p and ctCdc50p (grey). The A domain is yellow in E1-ATP and blue in E2P. The N domain is red in E1-ATP and cyan in E2P. TM2 is purple in E1-ATP and TMs 1 and 2 are green in E2P. **b,** same as **a**, except the N domains are omitted for clarity. The motion distance of the A domain between the E1-ATP an E2P states is labeled. **c,** same as **a**, except the A domains are omitted. The movement of the N domain between the E1 and E2 states is indicated. **d,** same as **a**, except rotating by 90 degrees and the A and N domains are omitted to show the movements of TMs 1 and 2 between the E1-ATP and E2P states.

Fig. S7 Comparison of AMPPCP in different E1-ATP structures

a-d, AMPPCP conformations from different P-type ATPases are shown as sticks. The protein structures from which AMPPCP are extracted are labeled.

Fig. S8 Comparison of phospholipid binding at E2-site1 in ctDnf1p and hATP8A1

a, Lipid binding at E2-site1 of ctDnf1p. The protein is shown as tan ribbon representation. The density of the lipid is shown as a grey mesh. The lipid (green) and its interacting residues (tan) are shown as sticks. **b,** Lipid binding in the E2Pi-PL structure of hATP8A1 (PDB ID: 6K7M, EMDB number: 9941). The protein is colored purple. The lipid is yellow. **c,** Superimposition of the two lipid binding sites. The yellow arrow and green arrow indicate the extension directions of the lipid acyl chains in hATP8A1 and ctDnf1p, respectively.

Fig. S9 Comparison of E1-site1 among P4-ATPase structures

a, E1-site1 in ctDnf1p. The density of the possible phospholipid substrate is shown as a grey mesh. The conserved serine residue is labeled. **b-c,** same as in **a**, except showing scDrs2p and hATP8A1, respectively.

Fig. S10 Interaction of the two terminal segments of ctCdc50p with ctDnf1p on the cytoplasmic side.

The N-terminal and C-terminal segments of ctCdc50p are colored yellow. The rest of ctCdc50p is pink. The ctDnf1p fragments that interact with ctCdc50p are colored red. The rest of ctDnf1p is tan. Interacting segments and TMs are labeled.

Fig. S11 A common lipid binding site in E1-ATP and E2P

a-**b,** Lipid binding site in E1-ATP (**a**) and E2P (**b**). The density of the lipid is shown as grey meshes. The lipid molecules are shown as sticks. **c,** Electrostatic potential surfaces of E1-ATP (left) and E2P (right), showing the lipid binding environment. The lipid molecules are shown as sticks. The surfaces showing here are on the opposite side of the surfaces showing in Fig. 2**b** and **d**.

Fig. S12 Model of phospholipid flipping by P4-ATPases

a, Cartoon drawing of E1-ATP. Domains are labeled and colored as in Fig 1**a**. The membrane is colored grey. The lipid molecules with light green heads are arranged to show the distortion of bilayers. The lipid molecule with the dark green head represents a substrate that is entering the transport pathway via E1-site2. **b,** Cartoon drawing of E2P. The lipid substrate is trapped in E2-site1. **c,** As in **a**, with the lipid bound at E1-site1. **d,** As in **b**, but the lipid substrate has been flipped to the cytosolic leaflet and waits at E2-site2 to be released.

Fig. S13 The "hydrophobic gate" residue I554 in cfDnf1p

a, Top view of the I554 and its interacting residues in E2P. The interacting residues are shown as sticks. **b,** Top view of I554 in E1-ATP. TM4 is in the same orientation as it is in **a**.

Table S1 Cryo-EM data collection, refinement and validation statistics

	ctDnf1p-Cdc50p with AMPPCP (EMDB-0873) (PDB 6LCR)	ctDnf1p-Cdc50p with BeF_3^- (EMDB-0872) (PDB 6LCP)
Data collection and processing		
Magnification	130,000	130,000
Voltage (kV)	300	300
Electron exposure (e–/Å^2)	57.5	57.5
Defocus range (μm)	-1.0 to -2.0	-1.0 to 2.0
Pixel size (Å)	1.055	1.055
Symmetry imposed	C1	C1
Initial particle images (no.)	2,397,258	2,820,251
Final particle images (no.)	272,912	249,694
Map resolution (Å)	3.40	3.48
FSC threshold 0.143		
Map resolution range (Å)	3.3-8.2	3.3-7.8
Refinement		
Model resolution (Å)	3.4	3.5
Map sharpening B factor (Å^2)	-94	-84
Model composition		
Non-hydrogen atoms	11590	12406
Protein residues	1420	1514
Ligands	17	18
B factors (Å^2)		
Protein	41.2	50.0
Ligand	45.6	51.5
R.m.s. deviations		
Bond lengths (Å)	0.012	0.010
Bond angles (°)	1.055	1.088
Validation		
MolProbity score	2.16	2.35
Clashscore	15.5	18.1
Poor rotamers (%)	0.31	0.25
Ramachandran plot		
Favored (%)	89.8%	88.1%
Allowed (%)	10.2%	11.7%
Disallowed (%)	0%	0.2%

Fig S1

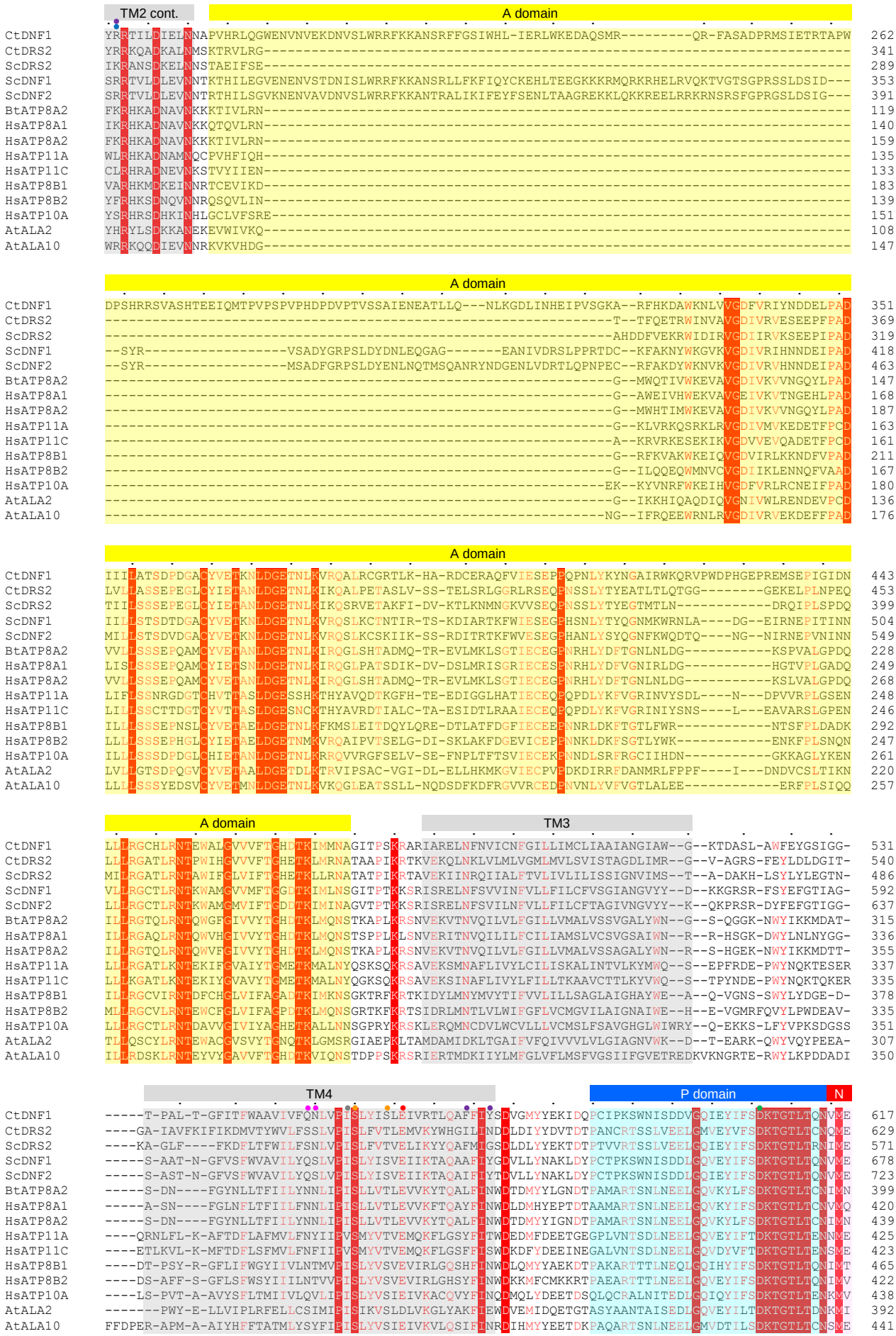
TM2 cont.
A domain
CtDNF1 262
CtDRS2 341
ScDRS2 289
ScDNF1 353
ScDNF2 391
BtATP8A2 119
HsATP8A1 140
HsATP8A2 159
HsATP11A 135
HsATP11C 133
HsATP8B1 183
HsATP8B2 139
HsATP10A 151
AtALA2 108
AtALA10 147
A domain
CtDNF1 351
CtDRS2 369
ScDRS2 319
ScDNF1 418
ScDNF2 463
BtATP8A2 147
HsATP8A1 168
HsATP8A2 187
HsATP11A 163
HsATP11C 161
HsATP8B1 211
HsATP8B2 167
HsATP10A 180
AtALA2 136
AtALA10 176
A domain
CtDNF1 443
CtDRS2 453
ScDRS2 399
ScDNF1 504
ScDNF2 549
BtATP8A2 228
HsATP8A1 249
HsATP8A2 268
HsATP11A 248
HsATP11C 246
HsATP8B1 292
HsATP8B2 247
HsATP10A 261
AtALA2 220
AtALA10 257
A domain
TM3
CtDNF1 531
CtDRS2 540
ScDRS2 486
ScDNF1 592
ScDNF2 637
BtATP8A2 315
HsATP8A1 336
HsATP8A2 355
HsATP11A 337
HsATP11C 335
HsATP8B1 378
HsATP8B2 335
HsATP10A 351
AtALA2 307
AtALA10 350
TM4
P domain
N
CtDNF1 617
CtDRS2 629
ScDRS2 571
ScDNF1 678
ScDNF2 723
BtATP8A2 399
HsATP8A1 420
HsATP8A2 439
HsATP11A 425
HsATP11C 423
HsATP8B1 465
HsATP8B2 422
HsATP10A 438
AtALA2 392
AtALA10 441


N domain
CtDNF1 669
CtDRS2 656
ScDRS2 598
ScDNF1 730
ScDNF2 775
BtATP8A2 427
HsATP8A1 448
HsATP8A2 467
HsATP11A 454
HsATP11C 451
HsATP8B1 496
HsATP8B2 456
HsATP10A 520
AtALA2 410
AtALA10 482
N domain
CtDNF1 724
CtDRS2 698
ScDRS2 641
ScDNF1 785
ScDNF2 830
BtATP8A2 475
HsATP8A1 495
HsATP8A2 515
HsATP11A 492
HsATP11C 484
HsATP8B1 541
HsATP8B2 501
HsATP10A 606
AtALA2 444
AtALA10 530
N domain
CtDNF1 738
CtDRS2 710
ScDRS2 653
ScDNF1 799
ScDNF2 844
BtATP8A2 486
HsATP8A1 506
HsATP8A2 526
HsATP11A 509
HsATP11C 499
HsATP8B1 553
HsATP8B2 513
HsATP10A 698
AtALA2 457
AtALA10 543
N domain
CtDNF1 817
CtDRS2 789
ScDRS2 734
ScDNF1 884
ScDNF2 929
BtATP8A2 565
HsATP8A1 585
HsATP8A2 605
HsATP11A 589
HsATP11C 579
HsATP8B1 632
HsATP8B2 592
HsATP10A 779
AtALA2 536
AtALA10 628
N domain
P
CtDNF1 902
CtDRS2 873
ScDRS2 818
ScDNF1 972
ScDNF2 1015
BtATP8A2 648
HsATP8A1 668
HsATP8A2 688
HsATP11A 670
HsATP11C 660
HsATP8B1 715
HsATP8B2 676
HsATP10A 872
AtALA2 619
AtALA10 713

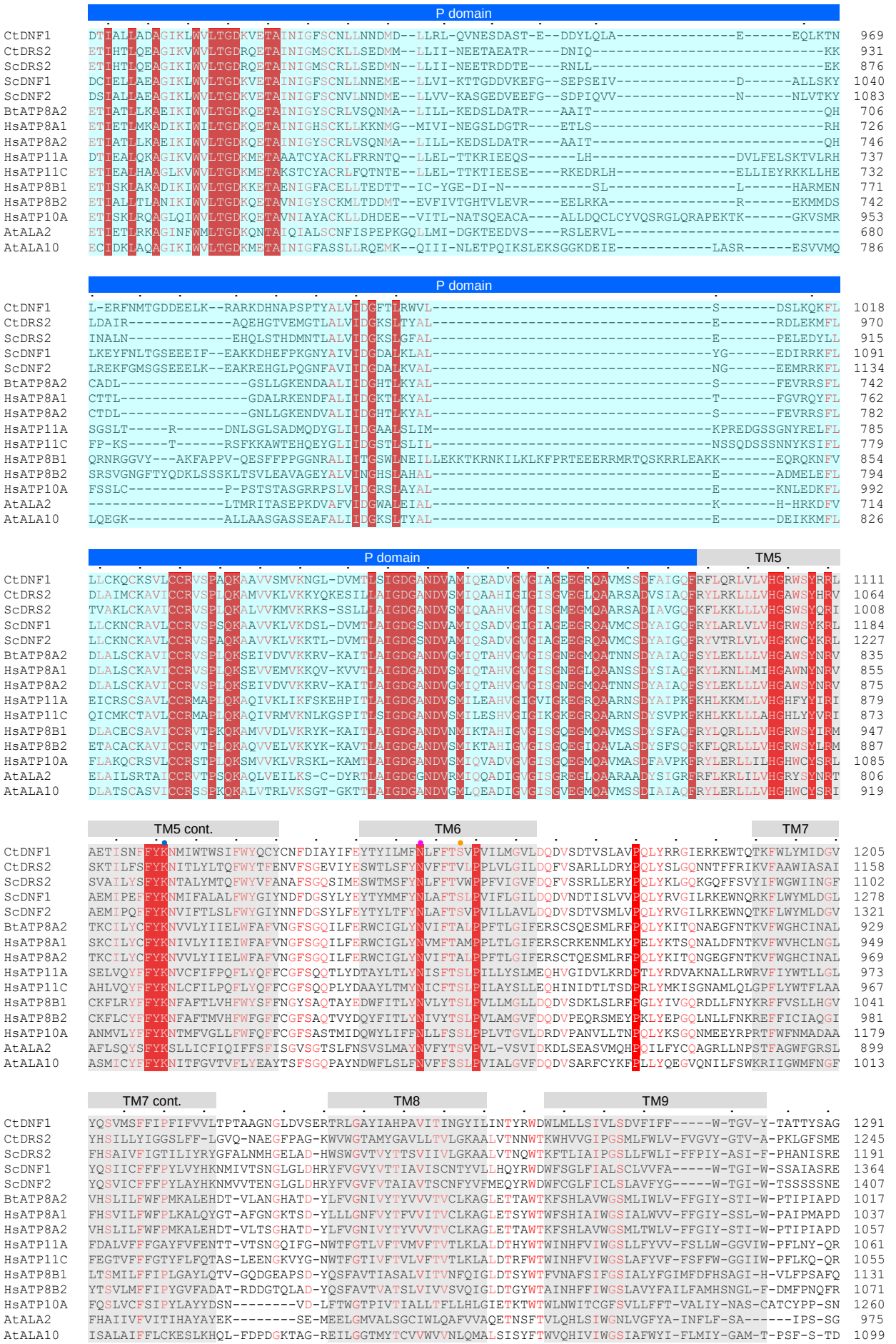
P domain
CtDNF1 969
CtDRS2 931
ScDRS2 876
ScDNF1 1040
ScDNF2 1083
BtATP8A2 706
HsATP8A1 726
HsATP8A2 746
HsATP11A 737
HsATP11C 732
HsATP8B1 771
HsATP8B2 742
HsATP10A 953
AtALA2 680
AtALA10 786
P domain
CtDNF1 1018
CtDRS2 970
ScDRS2 915
ScDNF1 1091
ScDNF2 1134
BtATP8A2 742
HsATP8A1 762
HsATP8A2 782
HsATP11A 785
HsATP11C 779
HsATP8B1 854
HsATP8B2 794
HsATP10A 992
AtALA2 714
AtALA10 826
P domain
TM5
CtDNF1 1111
CtDRS2 1064
ScDRS2 1008
ScDNF1 1184
ScDNF2 1227
BtATP8A2 835
HsATP8A1 855
HsATP8A2 875
HsATP11A 879
HsATP11C 873
HsATP8B1 947
HsATP8B2 887
HsATP10A 1085
AtALA2 806
AtALA10 919
TM5 cont.
TM6
TM7
CtDNF1 1205
CtDRS2 1158
ScDRS2 1102
ScDNF1 1278
ScDNF2 1321
BtATP8A2 929
HsATP8A1 949
HsATP8A2 969
HsATP11A 973
HsATP11C 967
HsATP8B1 1041
HsATP8B2 981
HsATP10A 1179
AtALA2 899
AtALA10 1013
TM7 cont.
TM8
TM9
CtDNF1 1291
CtDRS2 1245
ScDRS2 1191
ScDNF1 1364
ScDNF2 1407
BtATP8A2 1017
HsATP8A1 1037
HsATP8A2 1057
HsATP11A 1061
HsATP11C 1055
HsATP8B1 1131
HsATP8B2 1071
HsATP10A 1260
AtALA2 975
AtALA10 1099

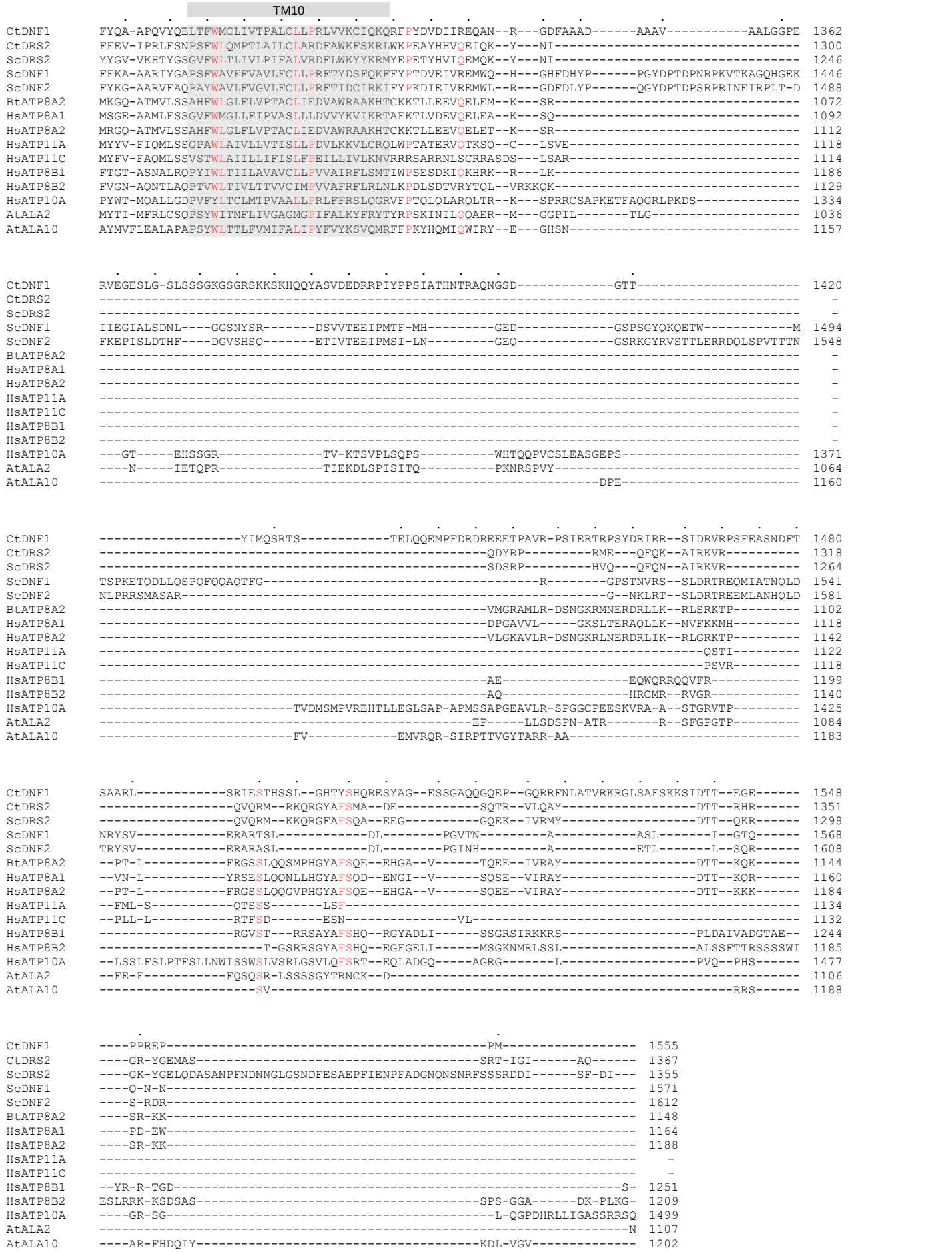
TM10
CtDNF1 FYQA-APQVYQELTFWMCLIVTPALCLLPRLVVKCIQKQRFPYDVDIIREQAN--R---GDFAAAD------AAAV----------AALGGPE 1362
CtDRS2 FFEV-IPRLFSNPSFWLQMPTLAILCLARDFAWKFSKRLWKPEAYHHVQEIQK--Y---NI---------- 1300
ScDRS2 YYGV-VKHTYGSGVFWLTLIVLPIFALVRDFLWKYYKRMYEPETYHVIQEMQK--Y---NI---------- 1246
ScDNF1 FFKA-AARIYGAPSFWAVFFVAVLFCLLPRFTYDSFQKFFYPTDVEIVREMWQ--H---GHFDHYP------PGYDPTDPNRPKVTKAGQHGEK 1446
ScDNF2 FYKG-AARVFAQPAYWAVLFVGVLFCLLPRFTIDCIRKIFYPKDIEIVREMWL--R---GDFDLYP------QGYDPTDPSRPRINEIRPLT-D 1488
BtATP8A2 MKGQ-ATMVLSSAHFWLGLFLVPTACLIEDVAWRAAKHTCKKTLLEEVQELEM--K---SR---------- 1072
HsATP8A1 MSGE-AAMLFSSGVFWMGLLFIPVASLLLDVVYKVIKRTAFKTLVDEVQELEA--K---SQ---------- 1092
HsATP8A2 MRGQ-ATMVLSSAHFWLGLFLVPTACLIEDVAWRAAKHTCKKTLLEEVQELET--K---SR---------- 1112
HsATP11A MYYV-FIQMLSSGPAWLAIVLLVTISLLPDVLKKVLCRQLWPTATERVQTKSQ--C---LSVE---------- 1118
HsATP11C MYFV-FAQMLSSVSTWLAIILLIFISLFPEILLIVLKNVRRRSARRNLSCRRASDS---LSAR---------- 1114
HsATP8B1 FTGT-ASNALRQPYIWLTIILAVAVCLLPVVAIRFLSMTIWPSESDKIQKHRK--R---LK---------- 1186
HsATP8B2 FVGN-AQNTLAQPTVWLTIVLTTVVCIMPVVAFRFLRLNLKPDLSDTVRYTQL--VRKKQK---------- 1129
HsATP10A PYWT-MQALLGDPVFYLTCLMTPVAALLPRLFFRSLQGRVFPTQLQLARQLTR--K---SPRRCSAPKETFAQGRLPKDS---------- 1334
AtALA2 MYTI-MFRLCSQPSYWITMFLIVGAGMGPIFALKYFRYTYRPSKINILQQAER--M---GGPIL-------TLG---------- 1036
AtALA10 AYMVFLEALAPAPSYWLTTLFVMIFALIPYFVYKSVQMRFFPKYHQMIQWIRY--E---GHSN---------- 1157
CtDNF1 RVEGESLG-SLSSSGKGSGRSKKSKHQQYASVDEDRRPIYPPSIATHNTRAQNGSD----------GTT---------- 1420
CtDRS2 ---------- -
ScDRS2 ---------- -
ScDNF1 IIEGIALSDNL----GGSNYSR-------DSVVTEEIPMTF-MH---------GED----------GSPSGYQKQETW----------M 1494
ScDNF2 FKEPISLDTHF----DGVSHSQ-------ETIVTEEIPMSI-LN---------GEQ----------GSRKGYRVSTTLERRDQLSPVTTTN 1548
BtATP8A2 ---------- -
HsATP8A1 ---------- -
HsATP8A2 ---------- -
HsATP11A ---------- -
HsATP11C ---------- -
HsATP8B1 ---------- -
HsATP8B2 ---------- -
HsATP10A ---GT-----EHSSGR----------TV-KTSVPLSQPS----------WHTQQPVCSLEASGEPS---------- 1371
AtALA2 ----N-----IETQPR----------TIEKDLSPISITQ----------PKNRSPVY---------- 1064
AtALA10 ----------DPE---------- 1160
CtDNF1 ----------YIMQSRTS----------TELQQEMPFDRDREEETPAVR-PSIERTRPSYDRIRR--SIDRVRPSFEASNDFT 1480
CtDRS2 ----------QDYRP---------RME---QFQK--AIRKVR---------- 1318
ScDRS2 ----------SDSRP---------HVQ---QFQN--AIRKVR---------- 1264
ScDNF1 TSPKETQDLLQSPQFQQAQTFG----------R--------GPSTNVRS--SLDRTREQMIATNQLD 1541
ScDNF2 NLPRRSMASAR----------G--NKLRT--SLDRTREEMLANHQLD 1581
BtATP8A2 ----------VMGRAMLR-DSNGKRMNERDRLLK--RLSRKTP---------- 1102
HsATP8A1 ----------DPGAVVL-----GKSLTERAQLLK--NVFKKNH---------- 1118
HsATP8A2 ----------VLGKAVLR-DSNGKRLNERDRLIK--RLGRKTP---------- 1142
HsATP11A ----------QSTI--------- 1122
HsATP11C ----------PSVR--------- 1118
HsATP8B1 ----------AE----------EQWQRRQQVFR---------- 1199
HsATP8B2 ----------AQ----------HRCMR--RVGR---------- 1140
HsATP10A ----------TVDMSMPVREHTLLEGLSAP-APMSSAPGEAVLR-SPGGCPEESKVRA-A--STGRVTP--------- 1425
AtALA2 ----------EP-----LLSDSPN-ATR-------R--SFGPGTP--------- 1084
AtALA10 ----------FV----------EMVRQR-SIRPTTVGYTARR-AA---------- 1183
CtDNF1 SAARL----------SRIESTHSSL--GHTYSHQRESYAG--ESSGAQQGQEP--GQRRFNLATVRKRGLSAFSKKSIDTT--EGE------ 1548
CtDRS2 ----------QVQRM--RKQRGYAFSMA--DE----------SQTR--VLQAY----------DTT--RHR------ 1351
ScDRS2 ----------QVQRM--KKQRGFAFSQA--EEG----------GQEK--IVRMY----------DTT--QKR------ 1298
ScDNF1 NRYSV----------ERARTSL----------DL--------PGVTN---------A----------ASL-------I--GTQ------ 1568
ScDNF2 TRYSV----------ERARASL----------DL--------PGINH---------A----------ETL-------L--SQR------ 1608
BtATP8A2 --PT-L----------FRGSSLQQSMPHGYAFSQE--EHGA--V------TQEE--IVRAY----------DTT--KQK------ 1144
HsATP8A1 --VN-L----------YRSESLQQNLLHGYAFSQD--ENGI--V------SQSE--VIRAY----------DTT--KQR------ 1160
HsATP8A2 --PT-L----------FRGSSLQQGVPHGYAFSQE--EHGA--V------SQEE--VIRAY----------DTT--KKK------ 1184
HsATP11A --FML-S----------QTSSS-------LSF---------- 1134
HsATP11C --PLL-L----------RTFSD-------ESN----------VL---------- 1132
HsATP8B1 ----------RGVST---RRSAYAFSHQ--RGYADLI------SSGRSIRKKRS----------PLDAIVADGTAE-- 1244
HsATP8B2 ----------T-GSRRSGYAFSHQ--EGFGELI------MSGKNMRLSSL----------ALSSFTTRSSSSWI 1185
HsATP10A --LSSLFSLPTFSLLNWISSWSLVSRLGSVLQFSRT--EQLADGQ-----AGRG-------L----------PVQ--PHS------ 1477
AtALA2 --FE-F----------FQSQSR-LSSSSGYTRNCK--D---------- 1106
AtALA10 ----------SV----------RRS------ 1188
CtDNF1 ----PPREP----------PM---------- 1555
CtDRS2 ----GR-YGEMAS----------SRT-IGI------AQ------ 1367
ScDRS2 ----GK-YGELQDASANPFNDNNGLGSNDFESAEPFIENPFADGNQNSNRFSSSRDDI------SF-DI--- 1355
ScDNF1 ----Q-N-N---------- 1571
ScDNF2 ----S-RDR---------- 1612
BtATP8A2 ----SR-KK---------- 1148
HsATP8A1 ----PD-EW---------- 1164
HsATP8A2 ----SR-KK---------- 1188
HsATP11A ---------- -
HsATP11C ---------- -
HsATP8B1 --YR-R-TGD----------S- 1251
HsATP8B2 ESLRRK-KSDSAS----------SPS-GGA------DK-PLKG- 1209
HsATP10A ----GR-SG----------L-QGPDHRLLIGASSRRSQ 1499
AtALA2 ----------N 1107
AtALA10 ----AR-FHDQIY----------KDL-VGV---------- 1202

Fig S2

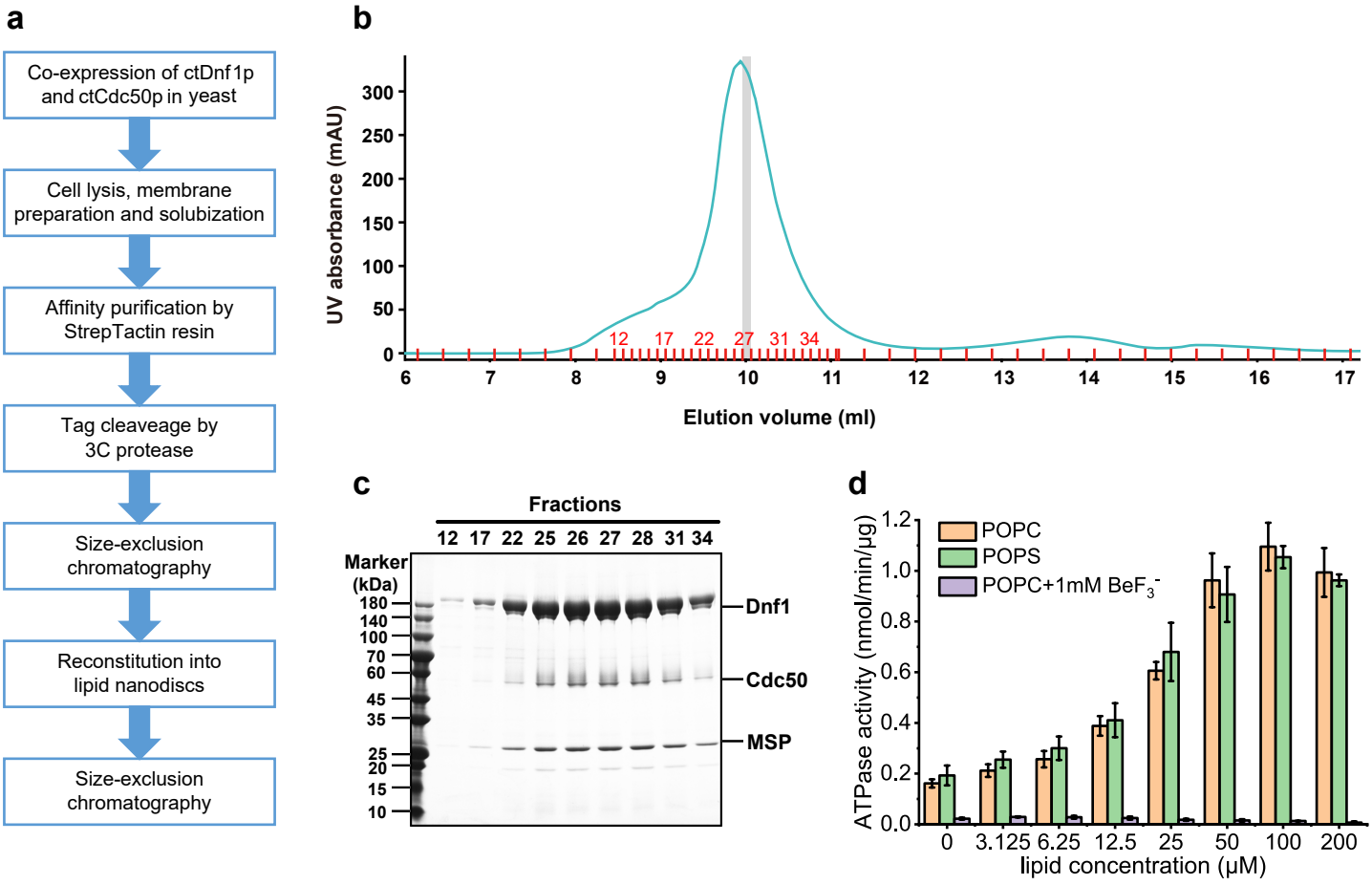
a
Co-expression of ctDnf1p and ctCdc50p in yeast
Cell lysis, membrane preparation and solubization
Affinity purification by StrepTactin resin
Tag cleaveage by 3C protease
Size-exclusion chromatography
Reconstitution into lipid nanodiscs
Size-exclusion chromatography
b
UV absorbance (mAU)
Elution volume (ml)
12 17 22 27 31 34
c
Fractions
12 17 22 25 26 27 28 31 34
Marker (kDa)
180
140
100
70
60
45
35
25
20
15
10
Dnf1
Cdc50
MSP
d
POPC
POPS
POPC+1mM BeF3-
ATPase activity (nmol/min/µg)
lipid concentration (µM)
0
3.125
6.25
12.5
25
50
100
200

Fig S3

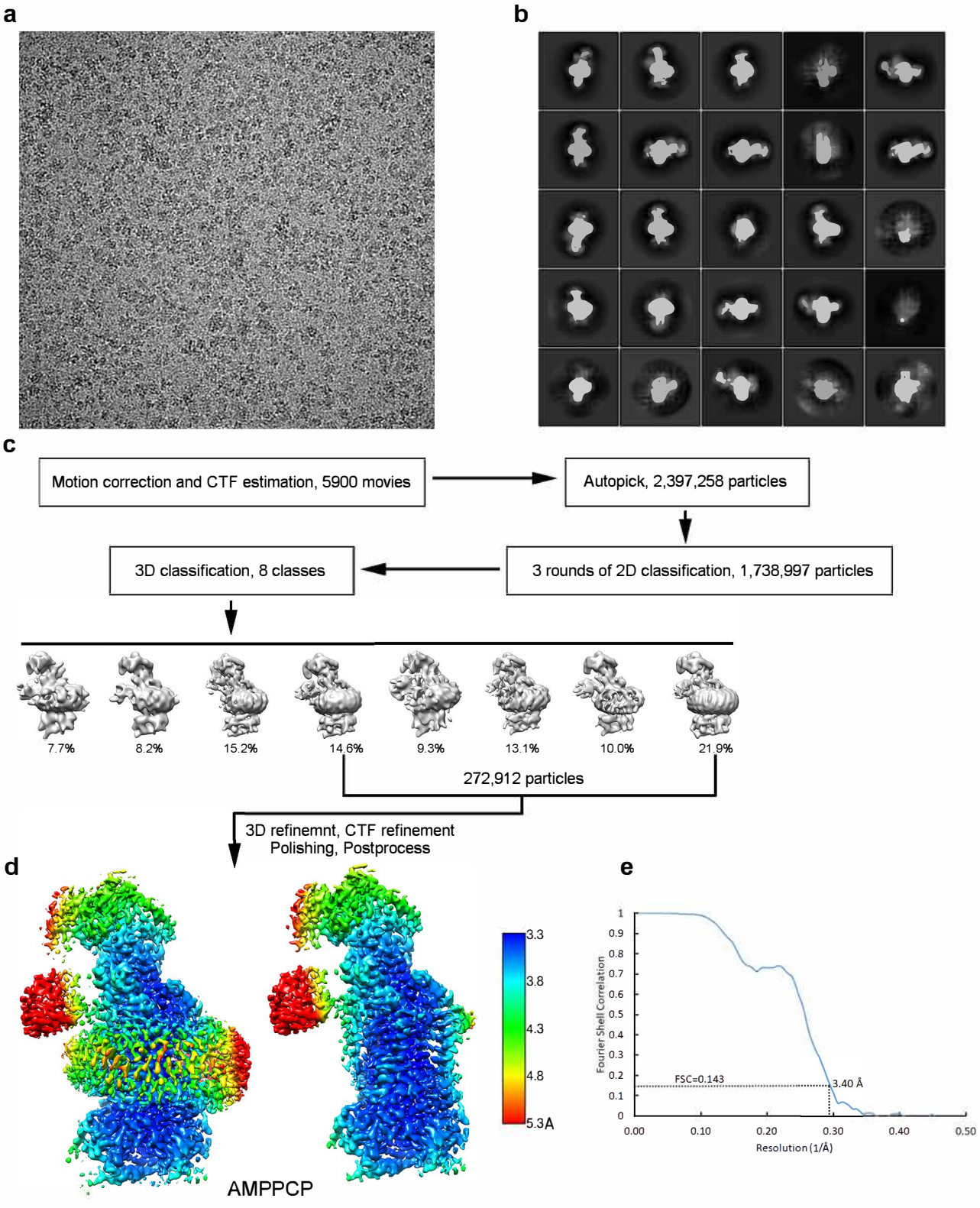
a
b
c
Motion correction and CTF estimation, 5900 movies
Autopick, 2,397,258 particles
3 rounds of 2D classification, 1,738,997 particles
3D classification, 8 classes
7.7%
8.2%
15.2%
14.6%
9.3%
13.1%
10.0%
21.9%
272,912 particles
3D refinemnt, CTF refinement
Polishing, Postprocess
d
3.3
3.8
4.3
4.8
5.3Å
AMPPCP
e
Fourier Shell Correlation
FSC=0.143
3.40 Å
Resolution (1/Å)

Fig. S4

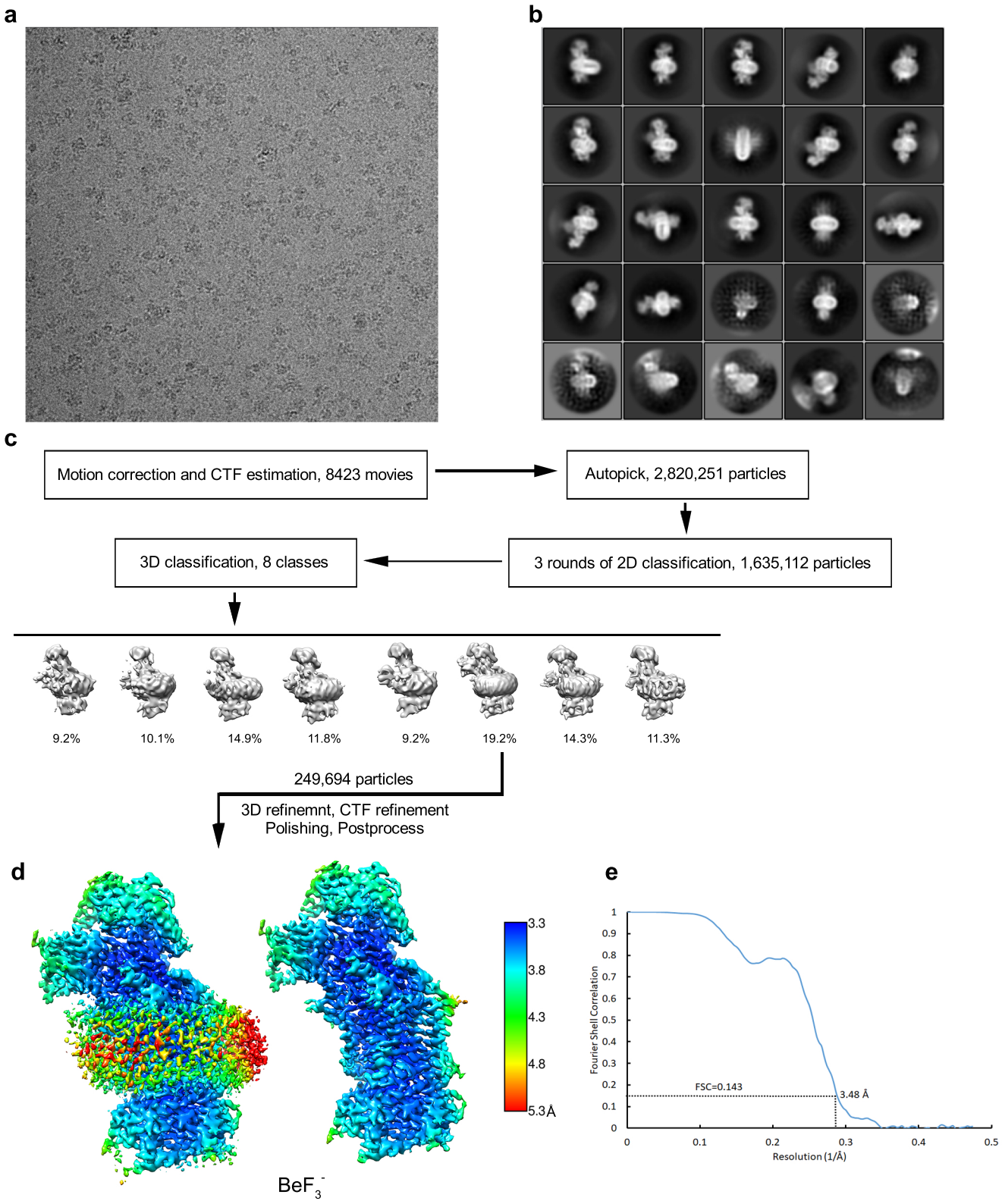
a
b
c
Motion correction and CTF estimation, 8423 movies
Autopick, 2,820,251 particles
3 rounds of 2D classification, 1,635,112 particles
3D classification, 8 classes
9.2%
10.1%
14.9%
11.8%
9.2%
19.2%
14.3%
11.3%
249,694 particles
3D refinemnt, CTF refinement
Polishing, Postprocess
d
3.3
3.8
4.3
4.8
5.3Å
BeF3-
e
Fourier Shell Correlation
FSC=0.143
3.48 Å
Resolution (1/Å)

Fig. S5

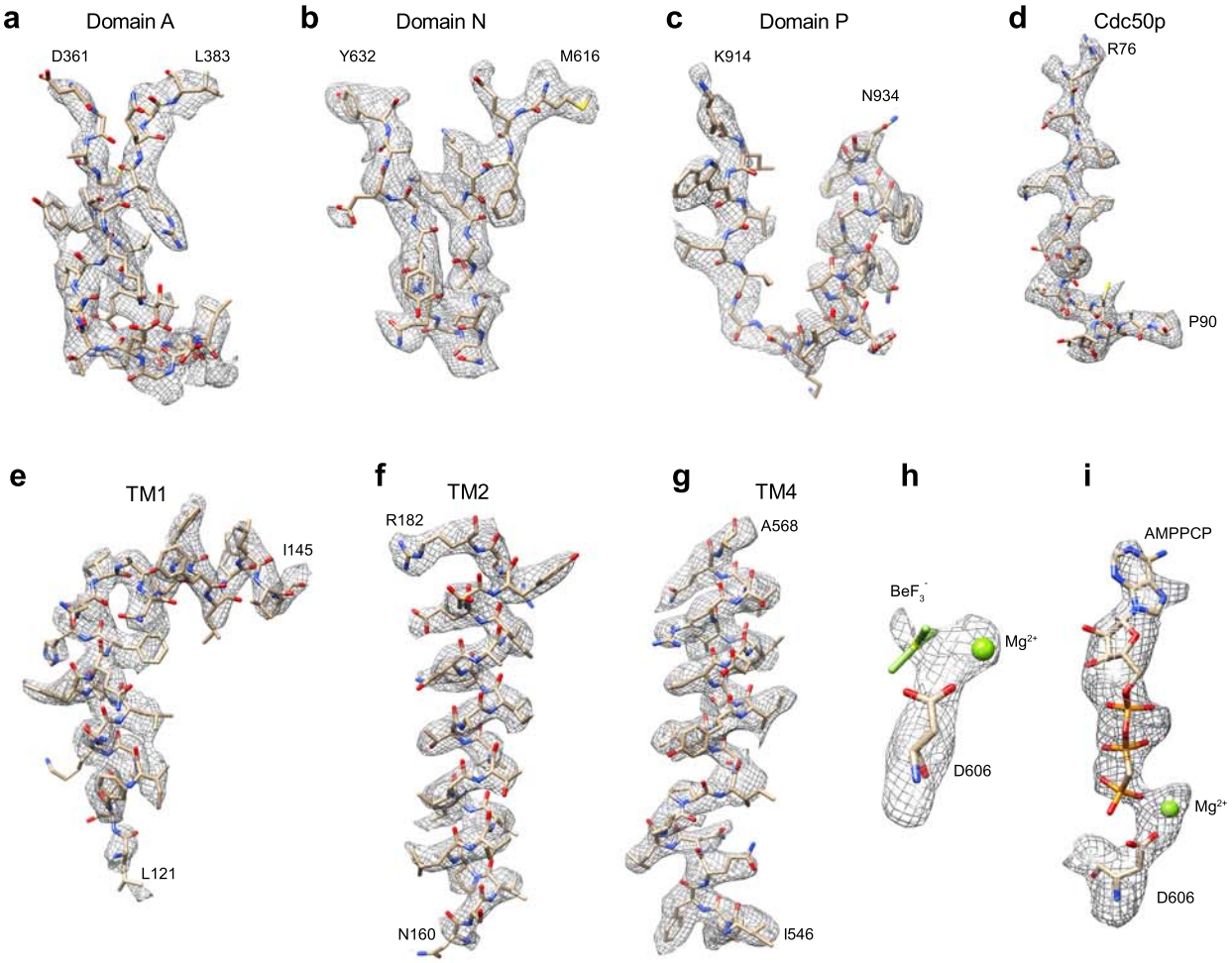
a
Domain A
D361
L383
b
Domain N
Y632
M616
c
Domain P
K914
N934
d
Cdc50p
R76
P90
e
TM1
I145
L121
f
TM2
R182
N160
g
TM4
A568
I546
h
BeF3-
Mg2+
D606
i
AMPPCP
Mg2+
D606

Fig. S6

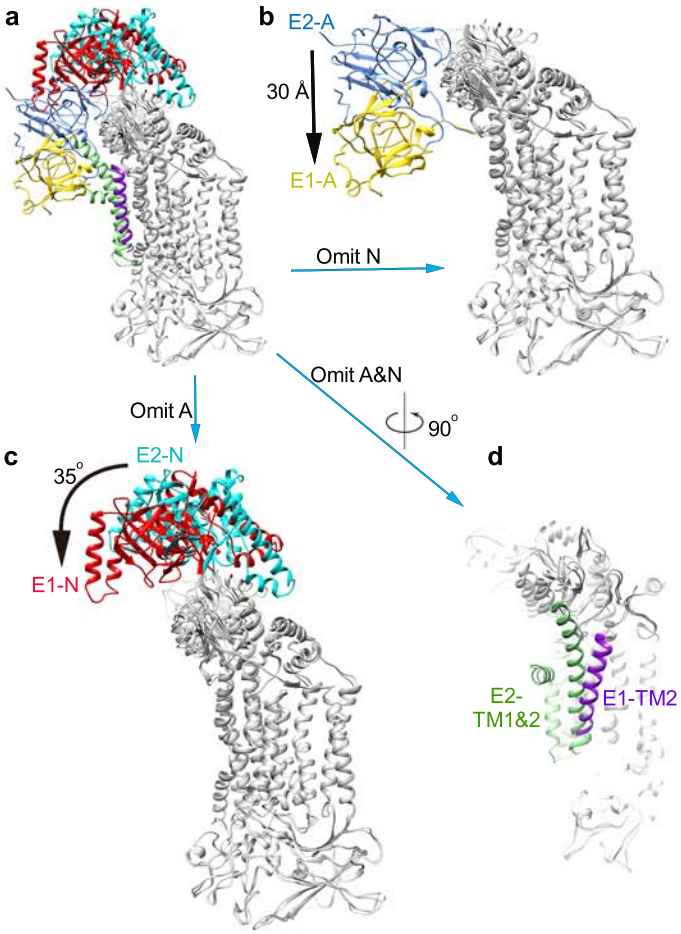
a
b
E2-A
30 Å
E1-A
Omit N
Omit A&N
90°
Omit A
c
35°
E2-N
E1-N
d
E2-
TM1&2
E1-TM2

Fig. S7

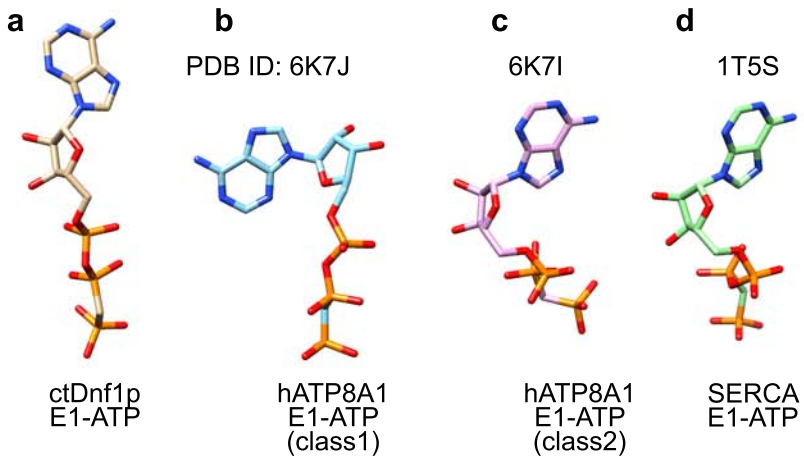
a
b
PDB ID: 6K7J
c
6K7I
d
1T5S
ctDnf1p
E1-ATP
hATP8A1
E1-ATP
(class1)
hATP8A1
E1-ATP
(class2)
SERCA
E1-ATP

Fig. S8

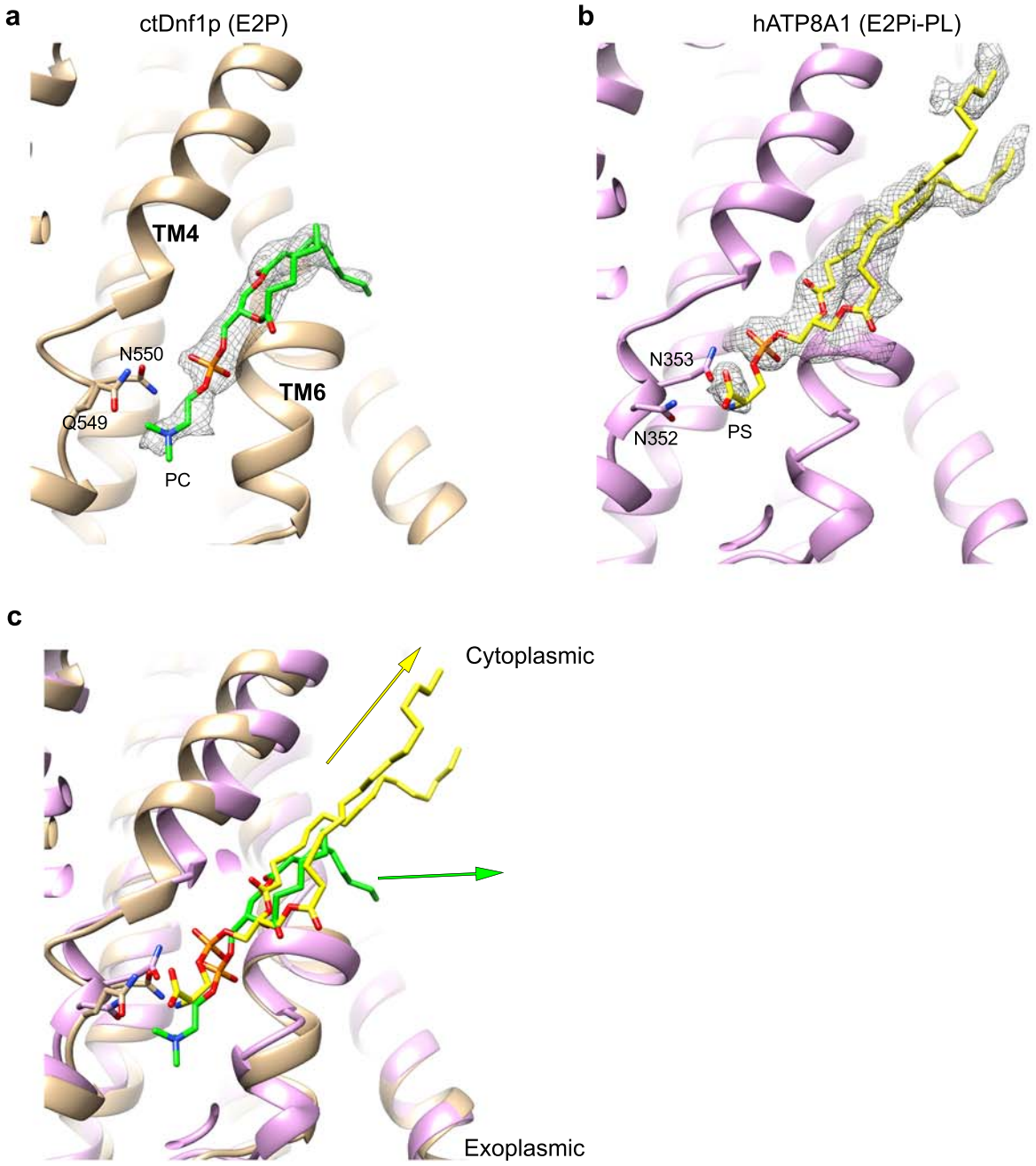
a
ctDnf1p (E2P)
TM4
N550
TM6
Q549
PC
b
hATP8A1 (E2Pi-PL)
N353
N352
PS
c
Cytoplasmic
Exoplasmic

Fig. S9

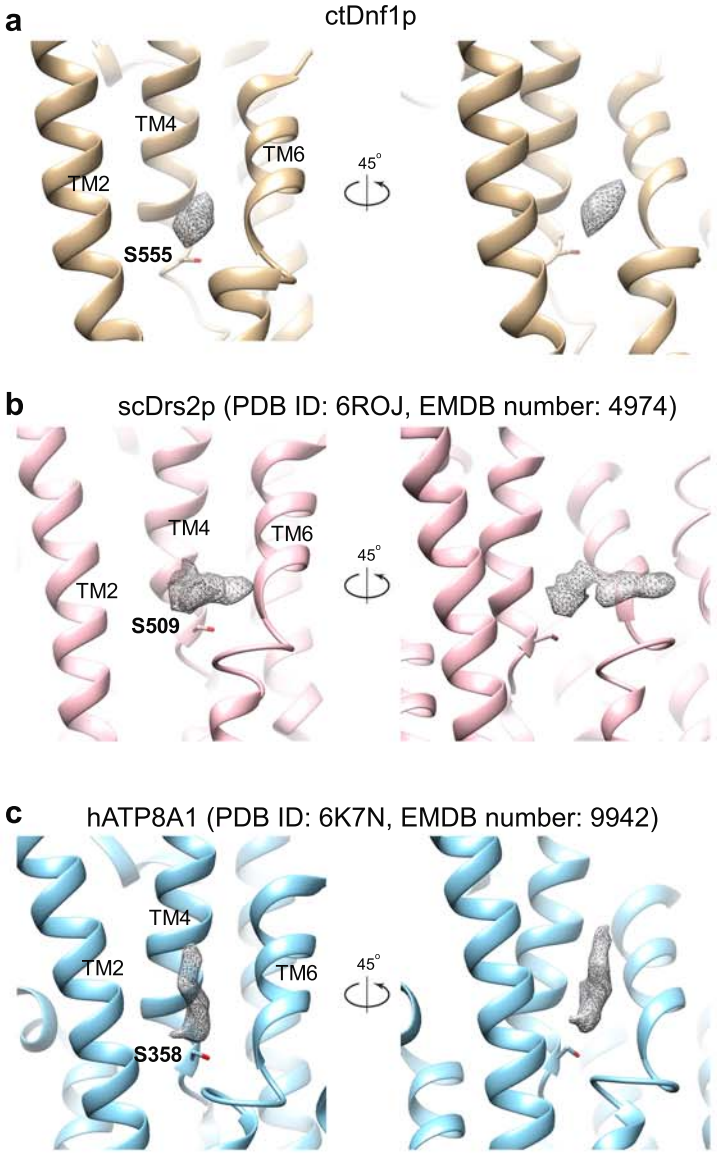
a
ctDnf1p
TM4
TM6
TM2
S555
45°
b
scDrs2p (PDB ID: 6ROJ, EMDB number: 4974)
TM4
TM6
TM2
S509
45°
c
hATP8A1 (PDB ID: 6K7N, EMDB number: 9942)
TM4
TM2
TM6
S358
45°

Fig. S10

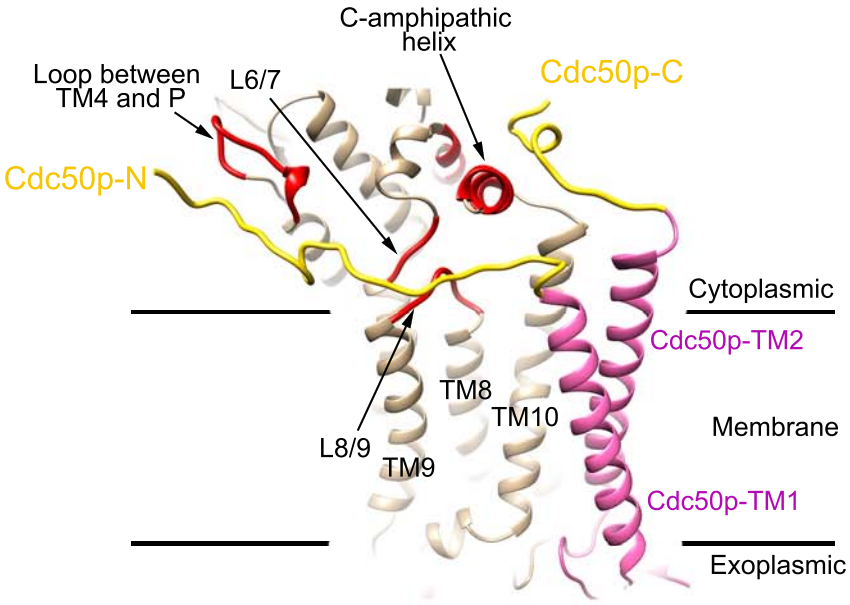
C-amphipathic
helix
Loop between
TM4 and P
L6/7
Cdc50p-C
Cdc50p-N
Cytoplasmic
Cdc50p-TM2
TM8
TM10
Membrane
L8/9
TM9
Cdc50p-TM1
Exoplasmic

Fig. S11

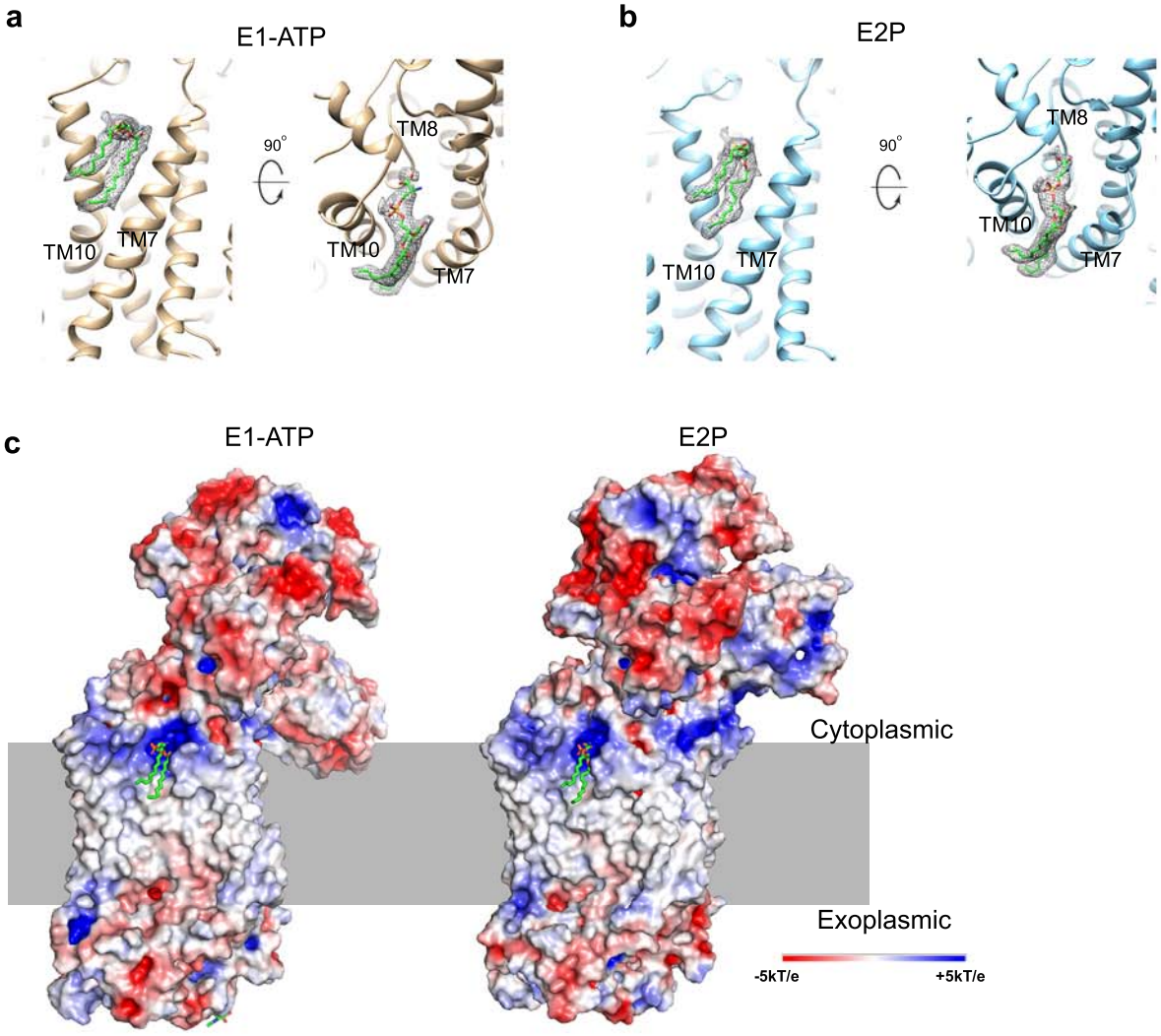
a
E1-ATP
TM10
TM7
90°
TM8
TM10
TM7
b
E2P
TM10
TM7
90°
TM8
TM10
TM7
c
E1-ATP
E2P
Cytoplasmic
Exoplasmic
-5kT/e
+5kT/e

Fig. S12

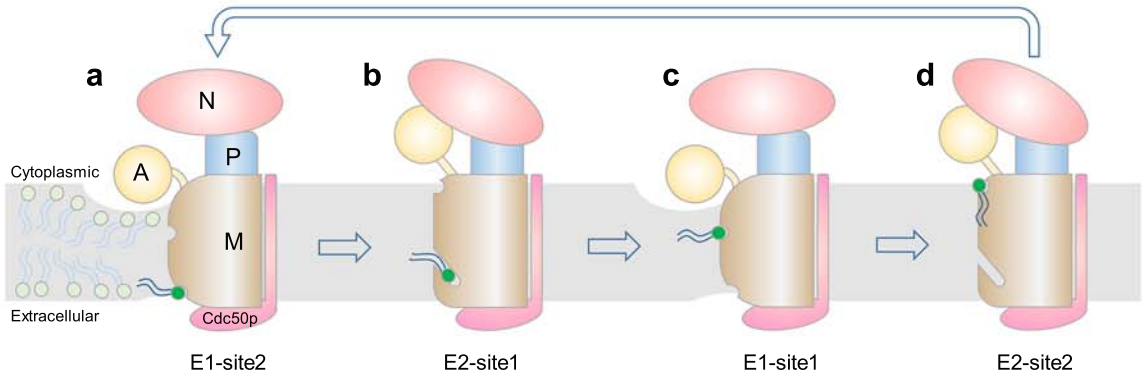
a
b
c
d
N
P
A
M
Cytoplasmic
Extracellular
Cdc50p
E1-site2
E2-site1
E1-site1
E2-site2

Fig. S13